Thermodynamical Structure of AdS Black Holes in Massive Gravity with Stringy Gauge-Gravity Corrections

S. H. Hendi[1,2*], B. Eslam Panah[1†], and S. Panahiyan[1,3 ‡]
[1] *Physics Department and Biruni Observatory, College of Sciences, Shiraz University, Shiraz 71454, Iran*
[2] *Research Institute for Astronomy and Astrophysics of Maragha (RIAAM), Maragha, Iran*
[3] *Physics Department, Shahid Beheshti University, Tehran 19839, Iran*

Motivated by gauge/gravity group in the low energy effective theory of the heterotic string theory, the minimal coupling of Gauss-Bonnet-massive gravity with Born-Infeld electrodynamics is considered. At first the metric function is calculated and then the geometrical properties of the solutions are investigated. It is found that there is an essential singularity at the origin and the intrinsic curvature is regular elsewhere. In addition, the effects of massive parameters on the horizons of black holes are studied and the conserved and thermodynamic quantities are calculated. Also, it is shown that the solutions satisfy the first law of thermodynamics. Furthermore using heat capacity of these black holes, thermal stability and phase transitions are investigated. The variation of different parameters and related modifications on the (number of) phase transition are examined. Next, the critical behavior of the Gauss-Bonnet-Born-Infeld-massive black holes in context of extended phase space is studied. It is shown that how the variation of the different parameters affects the existence and absence of phase transition. Also, it is found that for specific values of different parameters, these black holes may enjoy the existence of new type of phase transition which to our knowledge was not observed in black hole physics before.

arXiv:1510.00108v1 [hep-th] 1 Oct 2015

I. INTRODUCTION

This fact that the Universe expands with acceleration follows directly from the observation of high red-shift supernova [1] and indirectly from the measurement of angular fluctuations of cosmic microwave background fluctuations [2]. Since Einstein's theory can not explain current acceleration of the Universe, without fine tuning, various modified gravities have been proposed. For example one can refer to brane world cosmology [3, 4], scalar-tensor theories [5], $F(R)$ gravity theories [6, 7].

One of the interesting modified gravity is Lovelock gravity [8]. It is the most generalization that satisfies properties of Einstein's tensor in higher dimensions [8]. In addition, It was shown that there is an equivalency between field equation of the Lovelock gravity near an arbitrary null surface and a thermodynamic identity [9, 10]. Furthermore, by using field equation for Lovelock gravity, a relation between energy momentum tensor and thermodynamic features were found. On the other hand, evolution of the spacetime has been investigated by using degrees of freedom of bulk and surface in Lovelock gravity. It was also pointed out that considering Lovelock gravity provides a natural backdrop to test different conceptual and mathematical aspects of Einstein's theory [11]. Generalizations which are originated from Lovelock gravity enables us to obtain a better insight into the phenomena in Einstein's theory.

The first three terms of Lovelock gravity called Gauss-Bonnet (GB) gravity in presence of cosmological constant (GB gravity). The first term is the cosmological term and the second and third terms are the Einstein and second order Lovelock (GB) terms, respectively. The GB gravity has interesting properties which are listed below.

In order to have a ghost-free action, the quadratic curvature corrections to the Einstein-Hilbert action should be proportional to the GB term [12]. In addition, the natural next-to-leading order term of the heterotic string effective action which plays a fundamental role in Chern-Simons gravitational theories is GB term [13]. In Ref. [14], it was pointed out that considering GB gravity in addition to Einstein gravity will lead to obtaining modified Renyi entropies. These entropies violate specific inequality which must be hold for Renyi entropy. In addition, in case of AdS/CFT correspondence, it was shown that considering GB gravity will modify shear viscosity, entropy, thermal conductivity and electrical conductivity [15].

The existence of singularity at the origin for a point-like charge, represents a shortcoming of Maxwell theory. In order to overcome this problem, Born and Infeld in Ref. [16] generalized Maxwell theory to a nonlinear theory. This theory imposes a maximum strength of the electromagnetic field to resolve self-energy problem. The spherically symmetric solutions of Einstein gravity in presence of Born-Infeld (BI) theory was obtained in Ref. [17]. On the other hand, it was shown that BI theory could be derived in open super strings and D-branes in context of this theory are

* email address: hendi@shirazu.ac.ir
† email address: behzad_eslampanah@yahoo.com
‡ email address: ziexify@gmail.com

free from physical singularities [18]. For getting a better picture of properties of BI theory in string theory see Ref. [20]

In Einstein theory of gravity, gravitons are massless particles. In order to make a massive theory, one can simply add massive terms to Einstein gravity. This will lead to introduction of a massive theory with a massive spin 2 particle propagation in which for $m \to 0$, massless Einstein theory of gravity is recovered. Several types of massive gravity with their specific characteristics have been introduced and their properties have been investigated [21–26]. In Ref. [27] massive gravity is explored in more details. Another class of massive theory was introduced by Vegh in Ref. [28]. The black holes solutions of this theory in AdS spacetime has been investigated [29]. One of the interesting aspects of this theory is the lattice like behavior of the graviton in holographic conductor model. It was shown that limit of massless gravity leads to a Drude peak which approaches to delta function. This is the behavior of the lattice in theory of the field. In addition, this theory has been employed to study stability conditions and metal-insulator transition in AdS/CFT context [30, 36]. Several studies regarding thermodynamical aspects of the Vegh's massive gravity has been conducted [31–33]. In context of holography, the conductivity and phase transitions of these theories of massive gravity have been investigated [36]. In addition, the generalization to GB gravity and BI nonlinear electromagnetic fields were done. Their thermodynamical behavior have been investigated in details [34, 35]. In this paper, we consider these two generalization for gravity and matter field of the action and black holes in GB-BI-massive gravity.

Thermodynamical aspects of black holes plays a crucial role toward theory of quantum gravity [37]. Of the greatest interest is thermal stability of the black holes. In order to black holes be stable, thermal stability conditions indicate that the heat capacity must be positive valued. This is known as canonical ensemble. Investigation of the heat capacity also enables one to study the phase transitions of the black holes. It was pointed out that roots of the denominator and numerator of the heat capacity are denoted as two different types of the phase transition.

Recently, there has been a growing interest in considering cosmological constant as a thermodynamical variable. It was pointed out that this consideration will enrich thermodynamical structure [38] of the black holes and leads to removing ensemble dependency [39]. On the other hand, it was shown that interpretation of the negative cosmological constant as thermodynamical pressure may lead to a van der Waals like behavior of liquid/gas for black holes [40]. Consideration of the cosmological constant as a thermodynamical variable could be justified through AdS/CFT. In the first case, the Yang-Mills theory residing on the boundary of the AdS spacetime enjoys the existence of variation of color which is related to the variation of cosmological constant in the bulk spacetime [41]. In the second case, an RG-flow in context of field theory corresponds to extended phase space which is obtained by consideration of cosmological constant as thermodynamical variable [42]. In the space of the field theory, the way that number of degrees of freedom runs with the energy scale is codified by isotherm curves.

The paper is organized as follow. In Sec. II, GB-BI-massive gravity action and corresponding field equations will be introduced. Then, in Sec. III a class of black holes with this configuration is obtained and geometrical properties are investigated. Next, validation of the first law of thermodynamics is investigated through obtained thermodynamical and conserved quantities. Sec. V will be devoted to study thermal stability in canonical ensemble for GB-BI-massive black hole solutions. Next, we employ the analogy between cosmological constant and thermodynamical pressure in extended phase space and study critical behavior of the obtained solutions. We finish our paper with some concluding remarks.

II. BASIC EQUATIONS

The d-dimensional action of GB-massive gravity with a non-linear electrodynamics is

$$\mathcal{I} = -\frac{1}{16\pi}\int d^dx\sqrt{-g}\left(\mathcal{R} - 2\Lambda + \alpha L_{GB} + L(\mathcal{F}) + m^2\sum_i^4 c_i\mathcal{U}_i(g,f)\right), \tag{1}$$

where $\mathcal{R}$, Λ, m and α are the scalar curvature, the cosmological constant, the massive parameter and the coefficient of GB gravity, respectively, and L_{GB} is the Lagrangian of GB gravity

$$L_{GB} = R_{\mu\nu\gamma\delta}R^{\mu\nu\gamma\delta} - 4R_{\mu\nu}R^{\mu\nu} + R^2, \tag{2}$$

where $R_{\mu\nu}$ and $R_{\mu\nu\gamma\delta}$ are, respectively, the Ricci and the Riemann tensors. f is a fixed symmetric tensor, c_i's are constants and $\mathcal{U}_i$ are symmetric polynomials of the eigenvalues of the $d\times d$ matrix $\mathcal{K}^\mu_\nu = \sqrt{g^{\mu\alpha}f_{\alpha\nu}}$, which can be

written as

$$\mathcal{U}_1 = [\mathcal{K}], \tag{3}$$
$$\mathcal{U}_2 = [\mathcal{K}]^2 - [\mathcal{K}^2], \tag{4}$$
$$\mathcal{U}_3 = [\mathcal{K}]^3 - 3[\mathcal{K}][\mathcal{K}^2] + 2[\mathcal{K}^3], \tag{5}$$
$$\mathcal{U}_4 = [\mathcal{K}]^4 - 6[\mathcal{K}^2][\mathcal{K}]^2 + 8[\mathcal{K}^3][\mathcal{K}] + 3[\mathcal{K}^2]^2 - 6[\mathcal{K}^4]. \tag{6}$$

One of the primitive motivations of studying the BI theory is due to its relation to string effective actions. The functional form of BI Lagrangian $L(\mathcal{F})$ is presented by

$$L(\mathcal{F}) = 4\beta^2\left(1 - \sqrt{1 + \frac{\mathcal{F}}{2\beta^2}}\right), \tag{7}$$

where β and $\mathcal{F} = F_{\mu\nu}F^{\mu\nu}$ are the BI parameter and the Maxwell invariant, respectively, in which $F_{\mu\nu} = \partial_\mu A_\nu - \partial_\nu A_\mu$ is the electromagnetic field tensor and A_μ is the gauge potential. It is notable that, in the limit $\beta \to \infty$, Eq. (7) reduces to the standard Maxwell Lagrangian, as it should be.

Using the action (1) and variation of this action with respect to the metric tensor ($g_{\mu\nu}$) and the Faraday tensor ($F_{\mu\nu}$), one can obtain the following field equations

$$G_{\mu\nu} + \Lambda g_{\mu\nu} + H_{\mu\nu} - \frac{1}{2}g_{\mu\nu}L(\mathcal{F}) - \frac{2F_{\mu\lambda}F^{\lambda}_{\nu}}{\sqrt{1+\frac{\mathcal{F}}{2\beta^2}}} + m^2\chi_{\mu\nu} = 0, \tag{8}$$

$$\partial_\mu\left(\frac{\sqrt{-g}F^{\mu\nu}}{\sqrt{1+\frac{\mathcal{F}}{2\beta^2}}}\right) = 0, \tag{9}$$

in which $G_{\mu\nu}$ is the Einstein tensor, $H_{\mu\nu}$ and $\chi_{\mu\nu}$ are in the following forms

$$H_{\mu\nu} = -\frac{\alpha}{2}\left(8R^{\rho\sigma}R_{\mu\rho\nu\sigma} - 4R^{\rho\sigma\lambda}_{\mu}R_{\nu\rho\sigma\lambda} - 4RR_{\mu\nu} + 8R_{\mu\lambda}R^{\lambda}_{\nu} + g_{\mu\nu}L_{GB}\right), \tag{10}$$
$$\chi_{\mu\nu} = -\frac{c_1}{2}\left(\mathcal{U}_1 g_{\mu\nu} - \mathcal{K}_{\mu\nu}\right) - \frac{c_2}{2}\left(\mathcal{U}_2 g_{\mu\nu} - 2\mathcal{U}_1\mathcal{K}_{\mu\nu} + 2\mathcal{K}^2_{\mu\nu}\right) - \frac{c_3}{2}(\mathcal{U}_3 g_{\mu\nu} - 3\mathcal{U}_2\mathcal{K}_{\mu\nu} + 6\mathcal{U}_1\mathcal{K}^2_{\mu\nu} - 6\mathcal{K}^3_{\mu\nu}) - \frac{c_4}{2}(\mathcal{U}_4 g_{\mu\nu} - 4\mathcal{U}_3\mathcal{K}_{\mu\nu} + 12\mathcal{U}_2\mathcal{K}^2_{\mu\nu} - 24\mathcal{U}_1\mathcal{K}^3_{\mu\nu} + 24\mathcal{K}^4_{\mu\nu}). \tag{11}$$

III. GB-BI-MASSIVE BLACK HOLE SOLUTIONS

Here, we are looking for obtaining the topological static black holes. For this purpose, we consider the metric of d-dimensional spacetime as

$$ds^2 = -f(r)dt^2 + f^{-1}(r)dr^2 + r^2 h_{ij}dx_i dx_j, \quad i,j = 1,2,3,...,d-2, \tag{12}$$

in which $h_{ij}dx_i dx_j$ is the line element with constant curvature $(d-2)(d-3)\kappa$ and volume V_{d-2}. The constant κ is related to the boundary curvature and may has a positive (elliptic), negative (hyperbolic) or zero (flat) constant curvature.

Following [28], we consider the ansatz metric in the following form

$$f_{\mu\nu} = diag(0, 0, c^2 h_{ij}), \tag{13}$$

where c is positive constant. Considering Eq. (13), $\mathcal{U}_i$'s are [28]

$$\mathcal{U}_1 = \frac{d_2 c}{r}, \quad \mathcal{U}_2 = \frac{d_2 d_3 c^2}{r^2}, \quad \mathcal{U}_3 = \frac{d_2 d_3 d_4 c^3}{r^3}, \quad \mathcal{U}_4 = \frac{d_2 d_3 d_4 d_5 c^4}{r^4}, \tag{14}$$

where $d_i = d - i$. We use the gauge potential ansatz $A_\mu = h(r)\delta^0_\mu$ in Maxwell equation (9) to obtain electric field. Considering the metric (12), one can obtain

$$h(r) = -\sqrt{\frac{d_2}{2d_3}}\frac{q}{r^{d_3}}\ \mathcal{H}, \tag{15}$$

where $\mathcal{H}$ and Γ are

$$\mathcal{H} \ = \ hypergeom\left(\left[\frac{1}{2},\frac{d_3}{2d_2}\right],\left[\frac{3d_{7/3}}{2d_2}\right]-\eta\right), \tag{16}$$

$$\eta \ = \ \frac{d_2 d_3 q^2}{2\beta^2 r^{2d_2}}, \tag{17}$$

in which q is an integration constant which is related to the electric charge. In addition, the Maxwell equation implies that the electric field in d-dimensions is given by

$$F_{tr} = \frac{\sqrt{d_2 d_3}q}{r^{d_2}\sqrt{1+\eta}}. \tag{18}$$

Now, we obtain the topological static GB-BI black hole solutions in massive gravity. To do so, one may use any component of Eq. (8) and obtain metric function $f(r)$. It is a matter of calculation to show that rr and tt are the same, whereas, the $x_i x_i$ components of Eq. (8) are identical. Therefore, we write

$$\begin{aligned} e_{tt} \ = \ & 2\beta^2 f\left(1-\frac{1}{\Upsilon}\right)+\frac{f}{2r^4}\left\{d_2d_3d_4\alpha f\left[2rf'+d_5 f\right]-d_2d_3\kappa r^2\left[\frac{\alpha d_4 d_5\left(2f-\kappa\right)}{r^2}+\frac{2\alpha d_4 f'}{r}-1\right]\right. \\ & \left.-2\Lambda r^4-d_2\left[d_3 f+rf'\right]r^2+m^2\left[r^2 d_2\left(cc_1 r+d_3c^2c_2\right)+d_2d_3d_4\left(c^3c_3 r+d_5c^4c_4\right)\right]\right\}, \end{aligned} \tag{19}$$

$$\begin{aligned} e_{x_1x_1} \ = \ & 2r^2\beta^2\left[\Upsilon-1\right]-\frac{1}{2r^2}\left\{d_3d_4d_5\alpha f\left[4rf'+d_6 f\right]-r^4\left(2\Lambda+f''\right)+d_3d_4\left[2\alpha\left(f'^2+ff''\right)-f-\frac{2rf'}{d_4}\right]r^2\right. \\ & \left.-d_3d_4\kappa r^2\left[\frac{\alpha d_5 d_6\left(2f-\kappa\right)}{r^2}+\frac{4\alpha d_5 f'}{r}+2\alpha f''-1\right]+d_3m^2c\left[\left(c_1 r+d_4cc_2\right)r^2+d_4d_5c^2\left(c_3 r+d_6cc_4\right)\right]\right\} \end{aligned} \tag{20}$$

where f and h are functions of r and also $\Upsilon = \sqrt{1-\left(\frac{h'}{\beta}\right)^2}$. Using Eqs. (19) and (20), We can obtain the metric function as

$$\begin{aligned} f\left(r\right) \ = \ & \kappa+\frac{r^2}{2\alpha d_3 d_4}\left\{1-\sqrt{1+\frac{8\alpha d_3 d_4}{d_1 d_2}\left[\Lambda+\frac{d_1 d_2 m_0}{2r^{d_1}}+\mathcal{A}+\mathcal{B}\right]}\right\}, \\ \mathcal{A} \ = \ & -2\beta^2\left(1-\sqrt{1+\eta}\right)-\frac{d_2 q^2}{r^{2d_2}}\mathcal{H}, \\ \mathcal{B} \ = \ & -m^2 d_1^2 d_2^2\left[\frac{d_3 d_4 c^4 c_4}{2r^4}+\frac{d_3 c^3 c_3}{2r^3}+\frac{c^2 c_2}{2r^2}+\frac{cc_1}{2d_2 r}\right], \end{aligned} \tag{21}$$

where m_0 is integration constants which is related to the total mass of the black hole. It is notable that, the obtained metric function (21), satisfies all the components of Eq. (8).

In order to study the geometrical structure of this solution (21), we look for the essential singularity(ies). For this purpose, we calculate the Ricci and Kretschmann scalars and obtain following results

$$\lim_{r\longrightarrow 0} R \ \longrightarrow \ \infty, \tag{22}$$

$$\lim_{r\longrightarrow 0} R_{\alpha\beta\gamma\delta}R^{\alpha\beta\gamma\delta} \ \longrightarrow \ \infty, \tag{23}$$

the above results confirm that there is a curvature singularity at $r = 0$. On the other hand, in order to investigate the asymptotical behavior of the solutions, we find the curvature scalars at $r \longrightarrow \infty$. So we have

$$\lim_{r\longrightarrow\infty} R \ \longrightarrow \ \frac{dd_1\left(\sqrt{d_2^2+\frac{8d_2d_3d_4}{d_1}\alpha\Lambda}\right)}{2\alpha d_2 d_3 d_4}, \tag{24}$$

$$\lim_{r\longrightarrow\infty} R_{\alpha\beta\gamma\delta}R^{\alpha\beta\gamma\delta} \ \longrightarrow \ \frac{1}{d_3 d_4\alpha}\left[\frac{4\Lambda d_{-1}}{d_1}+\left(1+\frac{d_2 d_{-1}}{d_3 d_4\alpha}\right)\left(1-\sqrt{\frac{d_3}{d_1}+\frac{8\alpha\Lambda d_3 d_4}{d_1 d_2}}\right)\right]. \tag{25}$$

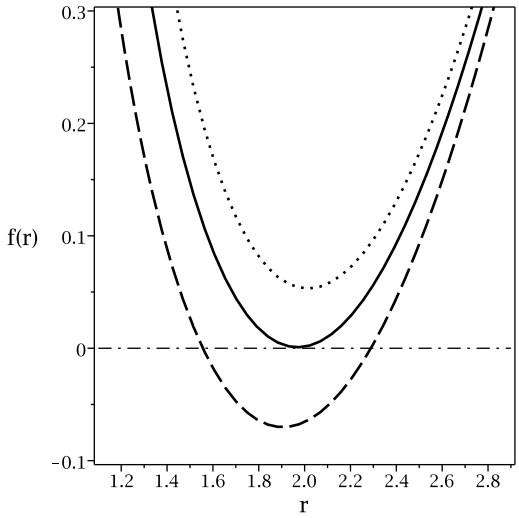

FIG. 1: $f(r)$ versus r for $\Lambda = -1$, $q = 1$, $\beta = 0.9$, $\alpha = 0.4$, $c = 1$, $c_1 = 0.3$, $c_2 = 1$, $c_3 = -4$, $c_4 = 2$, $m = 1$, $\kappa = 1$ and $d = 5$. $m_0 = 2.5$ (dashed line), $m_0 = 1.3$ (continues line) and $m_0 = 0.4$ (dotted line).

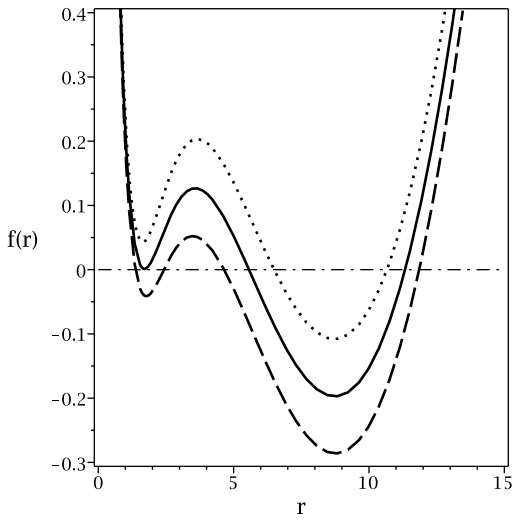

FIG. 2: $f(r)$ versus r for $\Lambda = -0.4$, $q = 1$, $\beta = 0.6$, $\alpha = 0.3$, $c = 0.8$, $c_1 = -2.1$, $m_0 = 3.1$, $c_3 = -4$, $c_4 = 1.9$, $m = 1.4$, $\kappa = 1$ and $d = 5$.
diagrams for $c_2 = 3.250$ (dashed line), $c_2 = 3.325$ (continues line) and $c_2 = 3.4$ (dotted line).

These results confirm that, the asymptotical behavior of the solutions are (a)dS solutions with an effective cosmological constant (Λ_{eff}). This effective cosmological constant reduces to ordinary Λ for vanishing α. In other words, neither massive nor BI parts affect the asymptotical behavior of the solutions.

It is worthwhile to mention that, in the absence of massive parameter ($m = 0$), the solution (21) reduces to d-dimensional asymptotically adS topological black hole solution which was found in Ref. [43]. In addition, for $\beta \longrightarrow \infty$, obtained solution reduces to GB-Massive solution with Maxwell field [34]. Moreover, for vanishing α the solution of Einstein-BI-massive gravity may be recovered [35].

In order to study the effects of the GB-BI-massive gravity on metric function, we have plotted the diagrams related to this solution in Figs. 1 and 2. The GB-BI-massive black holes may behave like Reissner-Nordström black holes. In other words, these black holes may contain two horizons (inner and outer horizons), one extreme horizon or without horizon (naked singularity) (see Fig. 1 for more details). On the other hand, by adjusting some of parameters, we may encounter with interesting behavior in which more than two horizons are observed (Figs. 2). The existence of three and four horizons for black holes is due to the presence of massive part of gravity [33–35].

IV. THERMODYNAMICS

In this section, we study thermodynamic properties of GB-BI-massive black holes. In order to examine the first law, we should calculate the conserved and thermodynamics quantities of the solutions in d-dimensions.

The Hawking temperature of these black holes can be obtained through the definition of surface gravity

$$\begin{aligned} T &= \frac{1}{4\pi\mathcal{N}}\left\{\frac{m^2}{r_+}\left[d_3d_4\left(c^3c_3r_+ + d_5c^4c_4\right) + r_+^2\left(cc_1r_+ + d_3c^2c_2\right)\right] + \frac{2r_+^3}{d_2}\left(2\beta^2 - \Lambda\right)\right. \\ &\left. -\frac{4\beta^2r_+^3}{d_2\Upsilon_+} + \frac{\kappa d_3}{r_+}\left(r_+^2 + \alpha\kappa d_4d_5\right)\right\}, \end{aligned} \tag{26}$$

where $\mathcal{N} = 2\alpha\kappa d_3d_4 + r_+^2$ and $\Upsilon_+ = \Upsilon\left|_{r=r_+}\right.$. Besides, using Gauss law, one can find the total electric charge of the black holes

$$Q = \frac{V_{d_2}\sqrt{d_2d_3}}{4\pi}q. \tag{27}$$

We obtain the electric potential at the horizon with respect to spacial infinity as reference

$$U = A_\mu\chi^\mu\left|_{r\to\infty}\right. - A_\mu\chi^\mu\left|_{r\to r_+}\right. = \sqrt{\frac{d_2}{2d_3}}\frac{q}{r_+^{d_3}}\,\mathcal{H}_+, \tag{28}$$

where $\mathcal{H}_+ = \mathcal{H}\left|_{r=r_+}\right.$. In order to obtain the entropy of the black holes (due to the existence of higher derivative gravity), one can use Wald's formula [45]. Calculations lead to

$$S = \frac{V_{d_2}}{4}r_+^{d_2}\left(1 + \frac{2d_2d_3}{r_+^2}\kappa\alpha\right), \tag{29}$$

which shows that area law is violated for GB-BI-massive black holes with non-flat horizons.

In addition, for obtaining the total finite mass of the black holes, one can use Hamiltonian approach which leads into following result

$$M = \frac{d_2\,V_{d_2}}{16\pi}m_0. \tag{30}$$

Having conserved and thermodynamic quantities, we are in a position to check the first law of thermodynamics. For this purpose, we obtain the mass (m_0) of Eqs. (30) and (21), as a function of other parameters

$$\begin{aligned} M(r_+,q) &= \frac{d_2\,V_{d_2}}{16\pi}\left\{d_3d_4\alpha\kappa^2r_+^{d_5} + \kappa r_+^{d_3} + \frac{2r_+^{d_1}}{d_1d_2}\left[2\beta^2\left(1 - \sqrt{1+\eta_+}\right) - \Lambda\right] + \frac{2d_2q^2}{d_1r_+^{d_3}}\mathcal{H}_+\right. \\ &\left. + \frac{m^2r_+^{d_5}}{d_2}\left[d_2d_3\left(c^3c_3r_+ + d_4c^4c_4\right) + r_+^2\left(cc_1r_+ + d_2c^2c_2\right)\right]\right\}, \end{aligned} \tag{31}$$

where $\eta_+ = \frac{d_2d_3q^2}{2\beta^2r_+^{2d_2}}$. Using Eq. (31), and by defining the temperature and the electric potential

$$T = \left(\frac{\partial M}{\partial r_+}\right)_Q\left(\frac{\partial r_+}{\partial S}\right)_Q \tag{32}$$

$$U = \left(\frac{\partial M}{\partial Q}\right)_S, \tag{33}$$

one finds that Eqs. (32) and (33) coincide with Eqs. (26) and (28), and therefore, we find that these thermodynamics quantities satisfy classical form of the first law of black hole thermodynamics

$$dM = TdS + UdQ. \tag{34}$$

V. HEAT CAPACITY AND STABILITY IN CANONICAL ENSEMBLE

Considering obtained conserved and thermodynamic quantities, we are in a position to study thermal stability of the solutions. There are different approaches for studying thermal stability which are in context of canonical and grand canonical ensembles. In grand canonical ensembles, by employing the mass of the black holes as a thermodynamical potential and its corresponding extensive parameters, one can build up the Hessian matrix. The stability is investigated by studying the behavior of the determinant of the Hessian matrix. The canonical ensemble approach is based on behavior of the heat capacity. In this paper, we will investigate the stability conditions in canonical ensemble. One can use following relation for calculating the heat capacity

$$C_Q = T\left(\frac{\partial T}{\partial S}\right)_Q^{-1}. \tag{35}$$

Using Eq. (26), we obtain $\left(\frac{\partial T}{\partial S}\right)_Q$ in the following form

$$\left(\frac{\partial T}{\partial S}\right)_Q = \frac{\kappa d_3\left(\mathcal{N}-2r_+^2\right)}{\pi d_2\mathcal{N}^3 r_+^{d_5}} + \frac{\left(3\mathcal{N}-2r_+^2\right)}{\pi d_2^2\mathcal{N}^3 r_+^{d_7}}\left(\frac{4\beta^2\left(\Upsilon_+-1\right)}{\Upsilon_+}-2\Lambda\right) - \frac{4h'h''}{\pi d_2^2\mathcal{N}^2 r_+^{d_8}\Upsilon_+^3} \tag{36}$$

$$-\frac{\alpha\kappa^2 d_3 d_4 d_5\left(\mathcal{N}+2r_+^2\right)}{\pi d_2\mathcal{N}^3 r_+^{d_3}} - \frac{2m^2\mathcal{E}}{\pi d_2\mathcal{N}^3 r_+^{d_3}}. \tag{37}$$

where $\mathcal{E}$ is

$$\mathcal{E} = d_3 d_4\left[d_5 c^4 c_4\left(r_+^2+\frac{\mathcal{N}}{2}\right)+c^3 c_3 r_+\right] + r_+^2\left[d_3 c^2 c_2\left(r_+^2-\frac{\mathcal{N}}{2}\right)+c c_1 r_+\left(r_+^2-\mathcal{N}\right)\right], \tag{38}$$

Eqs. (26) and (35) show that investigation of heat capacity in analytical form is not easy, and therefore, we plot T and C_Q to study their behaviors (see Figs. 3 - 8).

In the absence and small values of massive parameter, the temperature diagram has a minimum which is an increasing function of the massive parameter (Fig. 3 up panels). For sufficiently large enough massive parameter, the behavior of the temperature will be modified to having two minimums and one maximum (Fig. 3 up panels).

In the absence of GB parameter ($\alpha = 0$), a minimum is observed for temperature and for small values of it, similar to previous case, two minimums and one maximum are formed (Fig. 4 up panels). Interestingly, by increasing GB parameter (α), the number of extrema will be modified to only one minimum (Fig. 4 up panels).

In case of BI parameter, for strong nonlinearity parameter, the temperature starts from $-\infty$ and acquires root which was not observed in other two cases (Fig. 5 right panel). In previous cases, due to contributions of different parameters, there is a limitation for obtainable temperature whereas in case of strong nonlinearity parameter, this limitation is vanished. In addition, another extremum is formed for this case.

In case of topological effects on temperature, three different behaviors are observed. For flat horizon, a minimum for temperature is observed. Whereas for spherical symmetric, two minimums and one maximum are formed. Interestingly, in case of $\kappa = -1$, temperature enjoys the existence of a divergency and two extrema (Fig. 6 right panel).

The variation of dimensions has interesting effects. For 6 dimensions with specific values for different parameters, two minimums and one maximum exist, whereas, increasing dimensions to 7 leads to existence of one minimum (Fig. 7 right panel). In both of these cases, there is a lower limit for temperatures that system can acquire. Interestingly, for $d > 7$, the lower limit is vanished and the temperature starts from $-\infty$ with one root, one minimum and one maximum (Fig. 8 right panel). It is worthwhile to mention that for every dimensions, a horizon radius exists for every two set of dimensions in which temperature is same ($d \geq 5$).

It is notable that for temperature, in cases of one minimum, for every acquirable temperature except extremum, two horizon radii. Whereas in cases of two minimums and one maximum, for specific range of temperature, for every temperature, four or even five (for strong nonlinearity parameter) horizon radii exist. In addition, it should be pointed out that each extremum represents a divergency in heat capacity, hence phase transition point. The existence of root in temperature represents another type of phase transition. In cases of temperature with root, the non-physical solutions exist.

Now, we are interested in studying the stability conditions and phase transitions in canonical ensembles. As it was pointed out, the extrema are the places in which heat capacity meets divergencies. Therefore, according to number of the extremum in temperature, one can recognize number of phase transitions related to divergencies of heat capacity. The other phase transition points are related to the roots of the temperature, hence, heat capacity.

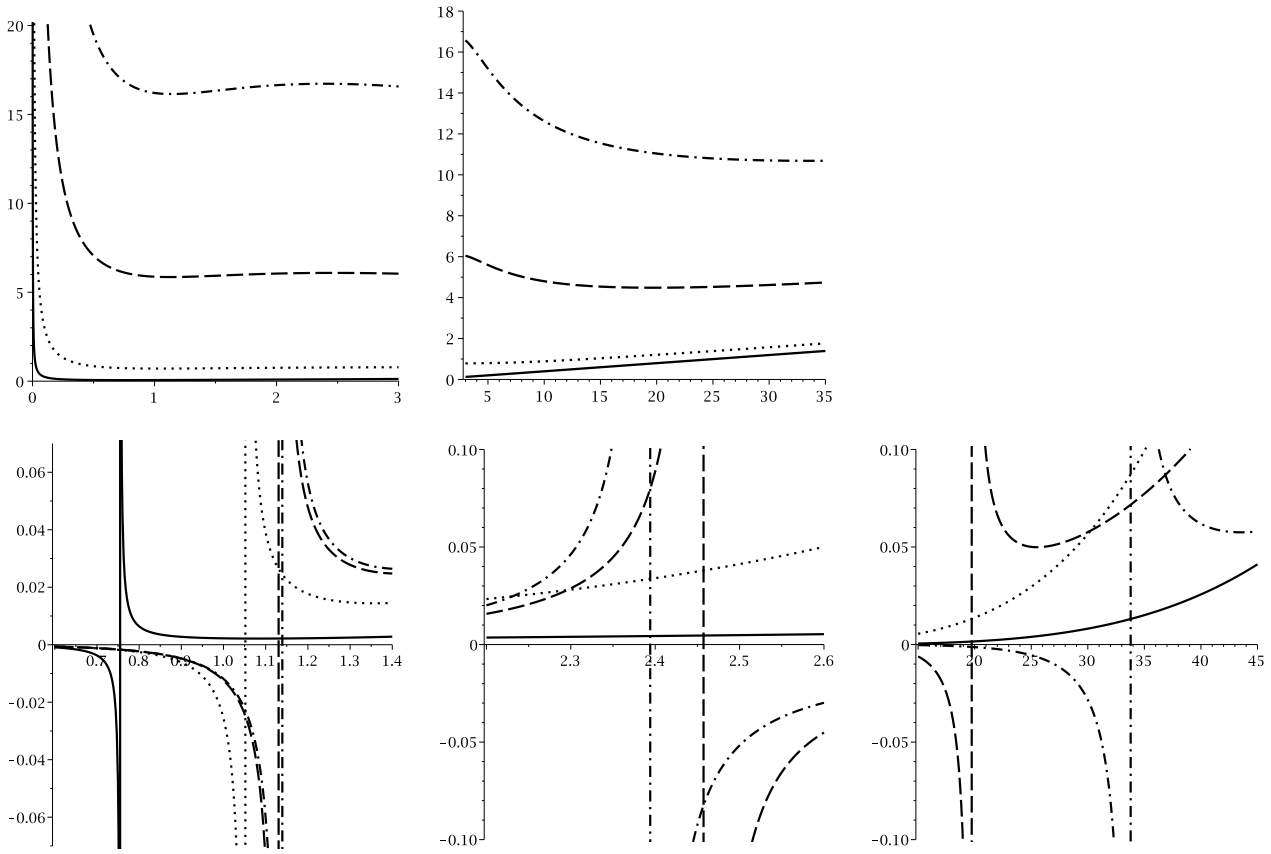

FIG. 3: For different scales: C_Q (down panels) and T (up panels) versus r_+ for $q = 1$, $\Lambda = -1$, $c = c_1 = c_2 = 2$, $c_3 = c_4 = 0.2$, $\beta = 0.5$, $\alpha = 0.5$, $d = 6$ and $\kappa = 1$; $m = 0$ (continues line), $m = 1$ (dotted line), $m = 3$ (dashed line) and $m = 5$ (dashes-dotted line).

According to what was mentioned, one can see that in case of small massive parameter (down panels of Fig. 3) and absence of α (down panels of Fig. 4), system only enjoys one phase transition of the smaller unstable to larger stable black holes. For sufficiently large enough massive parameter, system has three divergencies which are located at r_1, r_2 and r_3 where $r_1 < r_2 < r_3$ (down panels of Fig. 3). r_1 and r_3 are increasing functions of massive parameter and there is a phase transition of smaller unstable to larger stable black holes taking place in them, whereas r_2 is a decreasing function of massive parameter and has larger unstable to smaller stable black holes phase transition (see down panels of Fig. 3 for more details).

Interestingly, for specific range of α, three phase transitions exist for heat capacity (for more details see down panels of Fig. 4 for $\alpha = 0.5$ and $\alpha = 1$). In this case, r_1 and r_3 are decreasing functions of α, and r_2 is an increasing function of it with larger unstable to smaller stable and smaller unstable to larger stable black holes phase transitions, respectively. For large values of α, the number of the divergencies of the heat capacity and its type is similar to the absence of α.

In case of nonlinearity parameter, for small values of it, the black holes enjoy three phase transitions in their heat capacity in which r_1 is a decreasing, r_2 is an increasing functions of β and r_3 is independent of the variation of nonlinearity parameter. There are phase transitions of smaller unstable to larger stable black holes for r_1 and r_3 and vise versa for r_2. Increasing the nonlinearity parameter leads to formation of region of non-physical solutions (due to negativity of temperature) and additional phase transition point of stable non-physical to unstable physical phase transition. Also an extra divergency exists with phase transition of larger unstable to smaller stable black holes (for more details see Fig. 5).

In case of topological effects, flat horizon only has one smaller unstable to larger stable phase transition (two left panel of Fig. 6). Spherical horizon enjoys the existence of three phase transition points which was discussed before. Finally, for $\kappa = -1$, interestingly, due to existence of a divergency and extremum in temperature, black holes with this topological construction enjoy existences of the stable non-physical to unstable physical phase transition in place of divergency and smaller unstable to larger stable black holes phase transition in place of extremum (two left panel

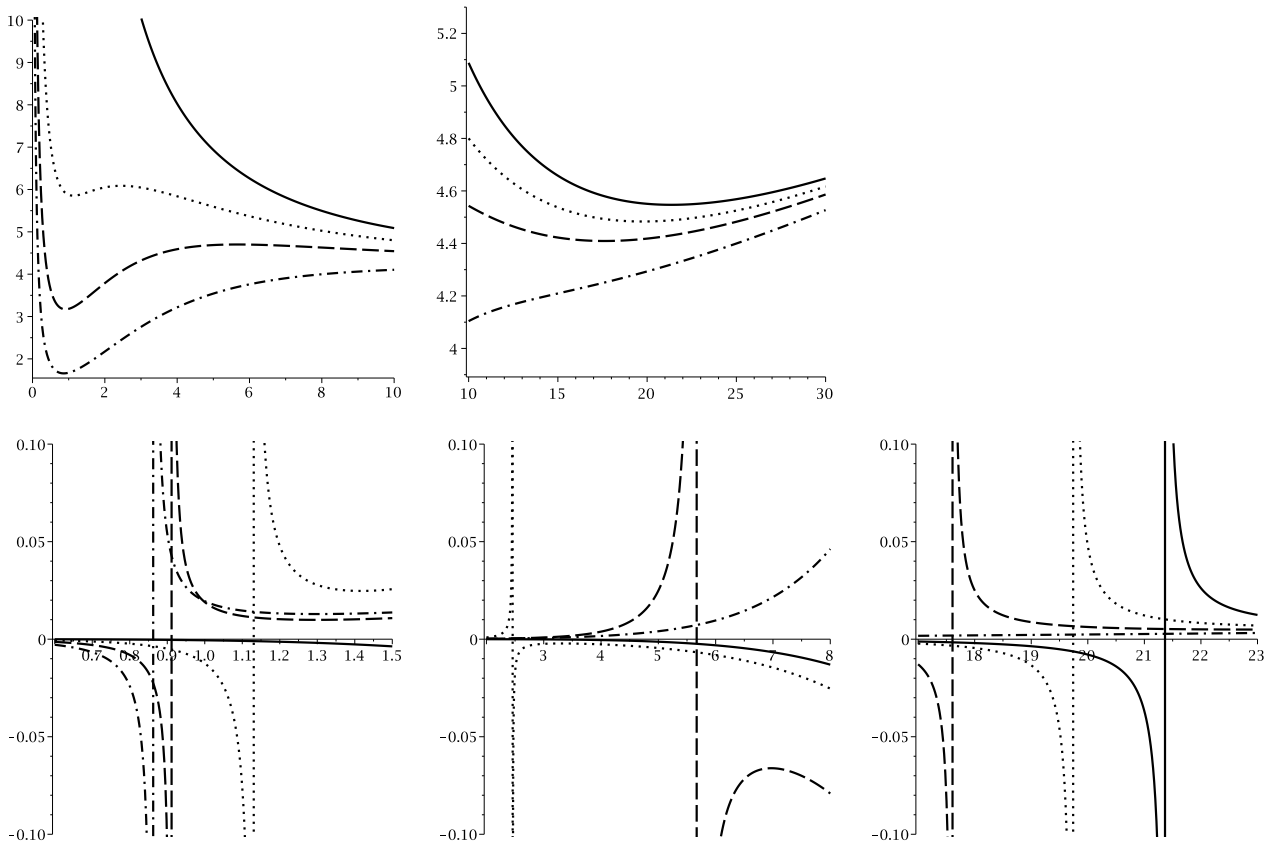

FIG. 4: For different scales: C_Q (down panels) and T (up panels) versus r_+ for $q = 1$, $\Lambda = -1$, $c = c_1 = c_2 = 2$, $c_3 = c_4 = 0.2$, $m = 3$, $\beta = 0.5$, $d = 6$ and $\kappa = 1$; $\alpha = 0$ (continues line), $\alpha = 0.5$ (dotted line), $\alpha = 1$ (dashed line) and $\alpha = 2$ (dashes-dotted line).

of Fig. 6). Interestingly, there is a case of extreme heat capacity for this topology.

Finally, for 6 dimensions, three divergencies exist for these black holes that was discussed before (Fig. 7). The case of 7 dimensions only enjoys one phase transition of smaller unstable to larger stable one (Fig. 7). Interestingly, for $d > 7$, due to modifications in temperature's behavior, two divergencies and one root exist (Fig. 8). In root, there is a phase transition of smaller unstable non-physical to larger stable physical. In place of smaller divergency, black holes go under phase transition of larger unstable to smaller stable black holes contrary to larger divergency. The divergencies are increasing functions of dimensions.

VI. $P - V$ CRITICALITY OF BLACK HOLE SOLUTIONS IN GB-BI-MASSIVE GRAVITY

In this section, we study the phase transition points of black holes in GB-BI-Massive gravity through the use of $P - V$ criticality and related phase diagrams in spherically symmetric spacetime ($\kappa = 1$). To do so, we consider following relationship between thermodynamical pressure and cosmological constant

$$P = -\frac{\Lambda}{8\pi}. \tag{39}$$

From thermodynamical point of view, one can point it out that conjugating thermodynamical variable corresponding to pressure would be thermodynamical volume. Therefore, in order to calculate the thermodynamical volume of the solutions, one should use

$$V = \left(\frac{\partial H}{\partial P}\right)_{S,Q}. \tag{40}$$

Considering cosmological constant as thermodynamical pressure leads to a interpretation of mass not only as internal energy but also as Enthalpy of thermodynamical system. This interpretation leads to following relation for the Gibbs

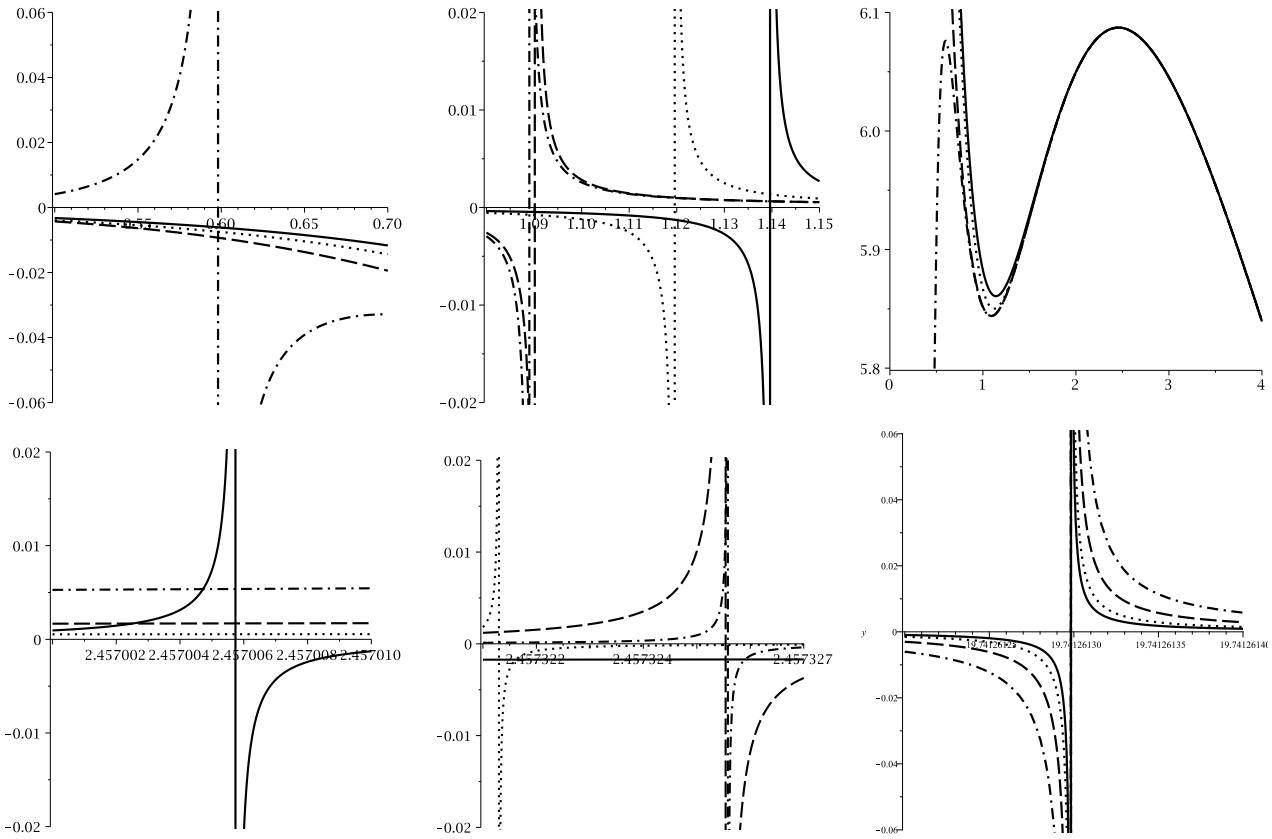

FIG. 5: For different scales: C_Q and T (only right up panel) versus r_+ for $q = 1$, $\Lambda = -1$, $c = c_1 = c_2 = 2$, $c_3 = c_4 = 0.2$, $m = 3$, $\alpha = 0.5$, $d = 6$ and $\kappa = 1$; $\beta = 0.1$ (continues line), $\beta = 1$ (dotted line), $\beta = 10$ (dashed line) and $\beta = 100$ (dashes-dotted line).

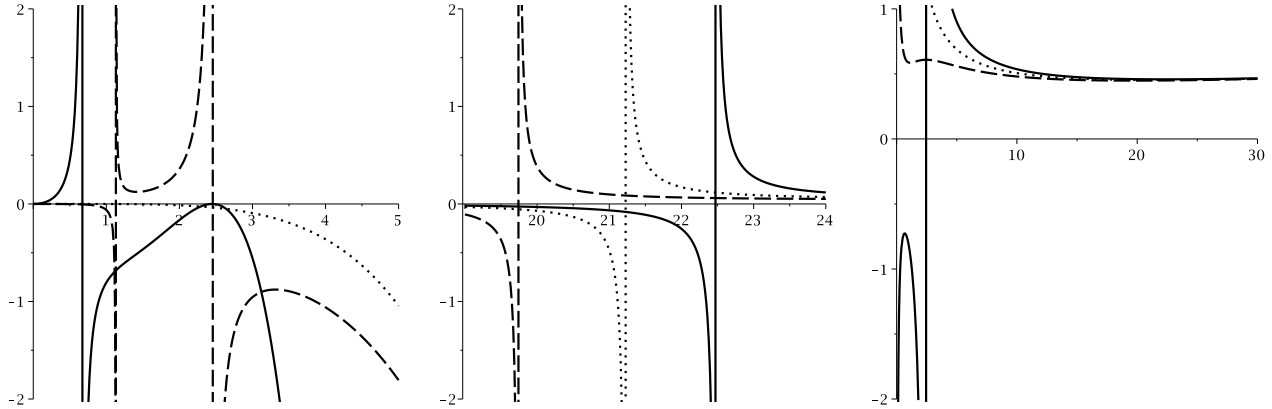

FIG. 6: For different scales: C_Q (left and middle panels) and T (right panel) versus r_+ for $q = 1$, $\Lambda = -1$, $c = c_1 = c_2 = 2$, $c_3 = c_4 = 0.2$, $m = 3$, $\beta = 0.5$, $d = 6$ and $\alpha = 0.5$; $\kappa = -1$ (continues line), $\kappa = 0$ (dotted line) and $\kappa = 1$ (dashed line).

free energy of the system

$$G = H - TS = M - TS, \tag{41}$$

There are several methods for studying the critical behavior of the system near critical points. Among them one can name $P-V$, $T-V$ and $G-T$ diagrams. The similarity that was observed in studying $P-V$ diagrams of black holes and van der Waals liquid/gas system, brought a new insight to black holes thermodynamics. $T-V$ diagrams enable one to investigate single state region of different phases for thermodynamical systems. In case of black holes, these single state of different regions are denoted as small and large black holes, which phase transitions take place between

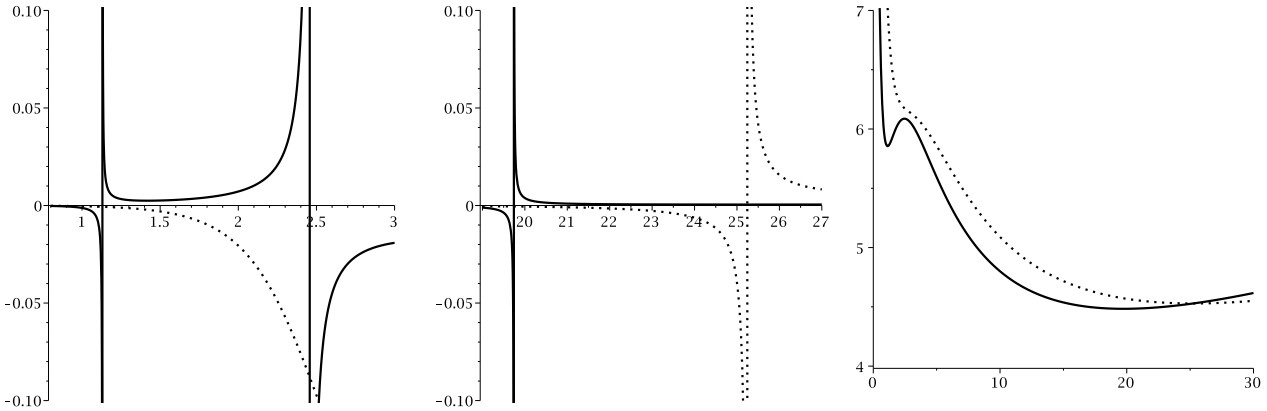

FIG. 7: For different scales: C_Q (left and middle panels) and T (right panel) versus r_+ for $q = 1$, $\Lambda = -1$, $c = c_1 = c_2 = 2$, $c_3 = c_4 = 0.2$, $m = 3$, $\beta = 0.5$, $\kappa = 1$ and $\alpha = 0.5$; $d = 6$ (continues line) and $d = 7$ (dotted line).

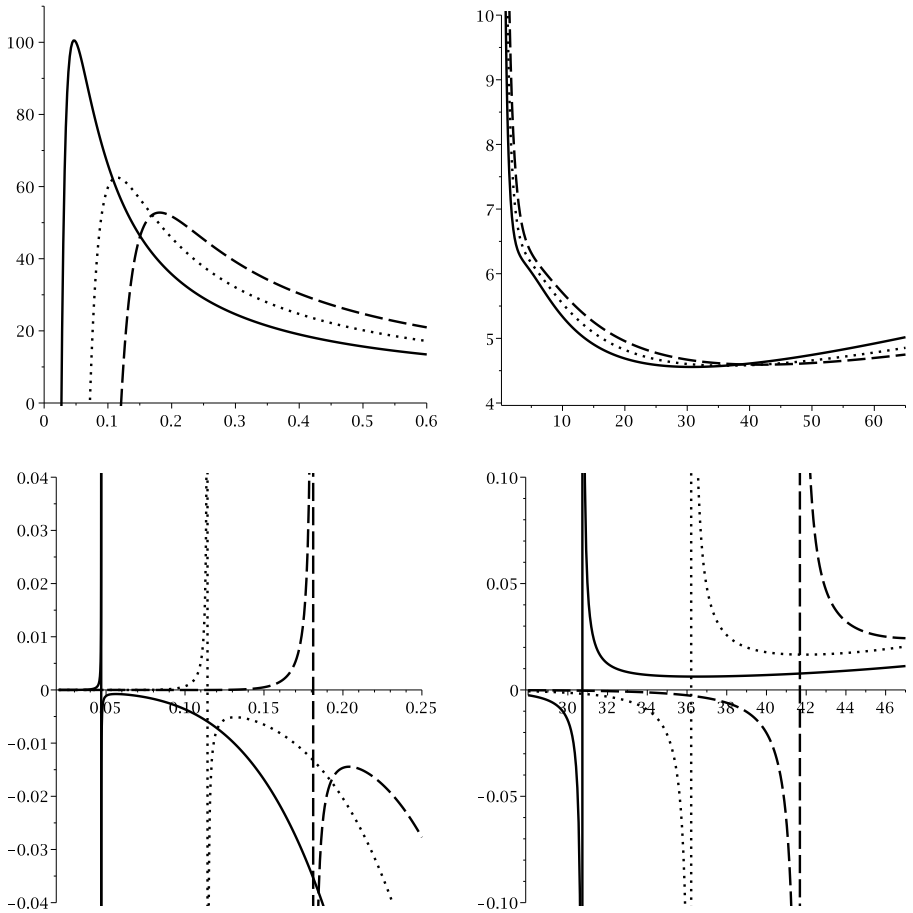

FIG. 8: For different scales: C_Q (down panels) and T (up panels) versus r_+ for $q = 1$, $\Lambda = -1$, $c = c_1 = c_2 = 2$, $c_3 = c_4 = 0.2$, $m = 3$, $\beta = 0.5$, $\kappa = 1$ and $\alpha = 0.5$; $d = 8$ (continues line), $d = 9$ (dotted line) and $d = 10$ (dashed).

them. The formation of the swallow-tail for pressures smaller than critical pressure, makes the $G - T$ diagrams one of the easiest ways for detecting a phase transition. According to what was mentioned, we will study critical behavior of these black holes by plotting $P - V$, $T - V$ and $G - T$ diagrams.

In order to find critical points, we use the inflection points that are obtainable through use of isotherm $P - V$ diagrams. We use following relations for obtaining critical values

$$\left(\frac{\partial P}{\partial r_+}\right)_T = \left(\frac{\partial^2 P}{\partial r_+^2}\right)_T = 0. \tag{42}$$

Using Eqs. (26), (29), (31), (39) and (41), one can find following relations for pressure and Gibbs free energy

$$\begin{aligned} P &= \frac{d_2\left(2\kappa\alpha' + r_+^2\right)T}{4r_+^3} - \frac{m^2 c d_2\left(d_3 d_4 c^2\left(d_5 c c_4 + c_3 r_+\right) + r_+^2\left(d_3 c c_2 + c_1 r_+\right)\right)}{16\pi r_+^4} \\ &+ \frac{\beta^2\left(\sqrt{1+\eta_+}-1\right)}{4\pi} - \frac{d_2\kappa\left(d_5\kappa\alpha' + d_3 r_+^2\right)}{16\pi r_+^4}, \end{aligned} \tag{43}$$

$$\begin{aligned} G &= \frac{d_2}{16\pi}\left[\kappa r_+^{d_3}\left(1+\frac{\kappa\alpha'}{r_+^2}\right) + \frac{m^2 c r_+^{d_5}\left(d_2 d_3 c^2\left(d_4 c c_4 + c_3 r_+\right) + r_+^2\left(d_2 c_2 c + c_1 r_+\right)\right)}{d_2}\right. \\ &+ \left.\frac{4r_+^{d_1}}{d_1 d_2}\left(\beta^2\left(1-\sqrt{1+\eta_+}\right)+4\pi P\right) + \frac{2d_2 q^2}{d_1 r_+^{d_3}}\mathcal{H}_+\right] - \frac{r_+^{d_2}\left(1+\frac{2d_2\kappa\alpha'}{d_4 r_+^2}\right)}{16\pi\left(2\kappa\alpha' + r_+^2\right)}\left[\frac{d_3\kappa\left(r_+^2 + \frac{d_5\kappa\alpha'}{d_3}\right)}{r_+}\right. \\ &+ \left.\frac{m^2 c\left(d_3 d_4 c^2\left(d_5 c c_4 + c_3 r_+\right) + r_+^2\left(d_3 c_2 c + c_1 r_+\right)\right)}{r_+} + \frac{4r_+^3}{d_2}\left(\beta^2\left(1-\sqrt{1+\eta_+}\right)+4\pi P\right)\right], \end{aligned} \tag{44}$$

where $\alpha' = d_3 d_4 \alpha$.
Now, by employing Eqs. (42) and (43), one can find following relation for calculating critical horizon radius

$$\begin{aligned} &\sqrt{2} r_+^{2d_2}\beta\sqrt{1+\eta_+}\left\{2\beta^2 d_3\left(\kappa + m^2 c_2 c^2\right) r_+^{2d-2} - 12 m^2 c r_+^{2d-3/2}\beta^2\left(c_1\kappa\alpha' - \frac{d_3 d_4 c_3 c^2}{2}\right) + 12 d_2 d_3 q^2 r_+^4 \mathcal{D}\right. \\ &\left. -24 r_+^{2d-1}\beta^2\left(\kappa^2\alpha' - \frac{d_3 d_4 d_5}{2} m^2 c_4 c^4 + \frac{d_3}{2} m^2 c_2 c^2 \kappa\alpha'\right) + 24 d_5 \kappa\alpha' r_+^{2d}\beta^2\left(\kappa^2\alpha' + d_3 d_4 m^2 c_4 c^4\right)\right\} \\ &-6\sqrt{2} d_2 d_3 q^2\beta\left[\frac{2d_{5/2}\beta^2}{3} r_+^{2d-3} + 4 d_{7/2}\kappa\alpha' r_+^{2d-2}\beta^2 + d_2 d_3 q^2 r_+^8\left(d\left(\kappa\alpha' + \frac{r_+^2}{6}\right) - \frac{r_+^2}{2} - 5\kappa\alpha'\right)\right] = 0 \end{aligned} \tag{45}$$

where $\mathcal{D}$ is

$$\begin{aligned} \mathcal{D} &= d_3 d_4 d_5 m^2 c_4 c^4\left(\kappa\alpha' + \frac{r_+^2}{2}\right) + \frac{d_3 d_4 m^2 c_3 c^3 r_+^3}{4} - \frac{d_3 m^2 c_2 c^2 r_+^2}{2}\left(\kappa\alpha' - \frac{r_+^2}{6}\right) - \frac{\kappa\alpha' m^2 c_1 c r_+^3}{2} \\ &+ \kappa\left(\frac{d_3 r_+^4}{12} - \kappa\alpha'\left(r_+^2 + d_5\kappa\alpha'\right)\right). \end{aligned} \tag{46}$$

m	r_c	T_c	P_c	$\frac{P_c r_c}{T_c}$
0.000000	2.020913551	0.1396519429	0.02602417127	0.3765976991
0.500000	2.378161673	0.4423844412	0.0555448739	0.2985970525
1.000000	2.518902071	1.3647986130	0.1515266147	0.2796608232
1.500000	2.555959475	2.9044194570	0.3125563944	0.2750571980
2.000000	2.570059221	5.0602917940	0.5381806700	0.2733352639

Table (1): $q = 1$, $\alpha = 0.5$, $\beta = 0.5$, $c = c_1 = c_2 = 2$, $c_3 = 0.2$, $c_4 = -0.2$ and $d = 6$.

β	r_c	T_c	P_c	$\frac{P_c r_c}{T_c}$
10^{-9}	2.308160166	0.4455199824	0.0568662372	0.2946139089
10^{-5}	2.308163661	0.4455195772	0.0568660973	0.2946138981
0.100000	2.352654221	0.4429849335	0.0558166578	0.2964373857
5.000000	2.379768359	0.4423515057	0.0555299142	0.2987405516
50.00000	2.379784726	0.4423511724	0.0555296666	0.2987414994
500.0000	2.379784890	0.4423511689	0.0555364292	0.2987779041
5000.000	2.379784892	0.4423511693	0.0552976969	0.2974935588

Table (2): $q = 1$, $m = 0.5$, $\alpha = 0.5$, $c = c_1 = c_2 = 2$, $c_3 = 0.2$, $c_4 = -0.2$ and $d = 6$.

α	r_c	T_c	P_c	$\frac{P_c r_c}{T_c}$
0.000000	1.655138693	0.7701822534	0.1684536184	0.3620105508
0.800000	2.745465406	0.3752283006	0.0381288304	0.2789805157
1.400000	3.430032297	0.3026420039	0.0223913368	0.2537751123
2.000000	4.066801555	0.2625706266	0.0152864154	0.2367622723
7.000000	0.4604432507	0.04557012100	−0.619424375	−6.258701240
	8.5661098700	0.16263006060	0.0032210312	0.1696593344
8.000000	0.6532944257	0.05173846074	−0.319158907	−4.029975610
	9.3813191800	0.15530428400	0.0026797563	0.1618735099
9.000000	0.7978966829	0.05408684451	−0.219549753	−3.238828615
	10.181225130	0.14928940340	0.0022720106	0.1549463726
400.00000	7.248776417	0.01324805968	−0.00684686743	−3.746315488
500.00000	7.933506025	0.01201916213	−0.00615425090	−4.062245443

Table (3): $q = 1$, $m = 0.5$, $\beta = 0.5$, $c = c_1 = c_2 = 2$, $c_3 = 0.2$, $c_4 = -0.2$ and $d = 6$.

It is evident that due to existence of the swallow-tail in $G-T$ diagrams for $P < P_c$, that system enjoys the existence of second order phase transition for specific values of different parameters (Fig. 9). The critical horizon radius is an increasing function of m, β and α. Whereas the critical temperature and pressure are increasing functions of massive parameter (Fig. 10 left and middle panels) and decreasing functions of GB (Fig. 11 right and middle panels) and nonlinearity (Fig. 12 left and middle panels) parameters. In addition, the ratio $\frac{P_c r_c}{T_c}$ is a decreasing function of the GB, massive and nonlinearity parameters.

On the other hand, the size of swallow-tail is an increasing function of the massive (Fig. 10 right panel) and GB (Fig. 11 right panel) parameters and is not highly a sensitive function of the β (Fig. 12 right panel). The length of subcritical isobars which is representing the phase transition region, is an increasing function of GB parameter (Fig. 11 middle panel) and a decreasing function of the massive parameter (Fig. 10 middle panel). It is worthwhile to mention, similar to the case of size of swallow-tail, the length of subcritical isobar is not changed considerably by variation of nonlinearity parameter (Fig. 12 middle panel).

It should be pointed out that for large values of nonlinearity parameter, the nonlinear strength will be weak and the behavior of the system will be Reissner-Nordström like. On the contrary, for sufficiently small values of nonlinearly

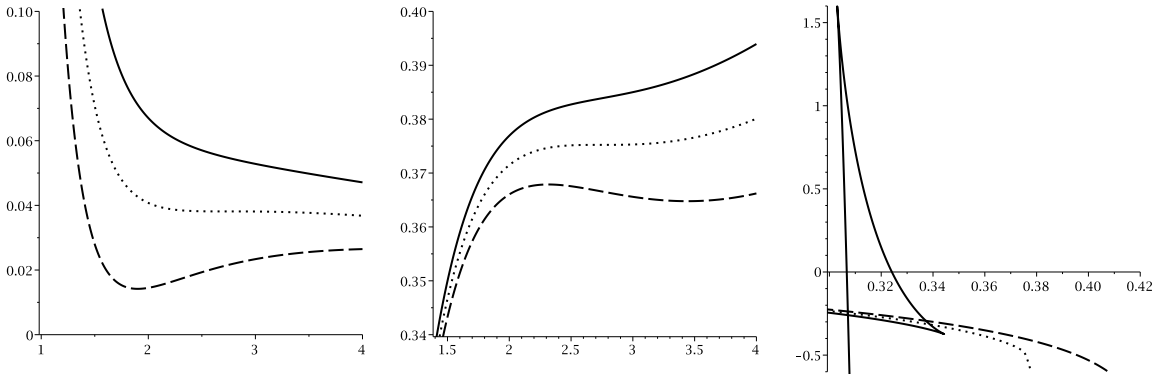

FIG. 9: $P - r_+$ (left), $T - r_+$ (middle) and $G - T$ (right) diagrams for $\beta = 0.5$, $q = 1$, $m = 0.5$, $\alpha = 0.8$, $c = c_1 = c_2 = 2$, $c_3 = 0.2$, $c_4 = -0.2$ and $d = 6$.
$P - r_+$ diagram, from up to bottom $T = 1.1T_c$, $T = T_c$ and $T = 0.9T_c$, respectively.
$T - r_+$ diagram, from up to bottom $P = 1.1P_c$, $P = P_c$ and $P = 0.9P_c$, respectively.
$G - T$ diagram for $P = 0.5P_c$ (continuous line), $P = P_c$ (dotted line) and $P = 1.5P_c$ (dashed line).

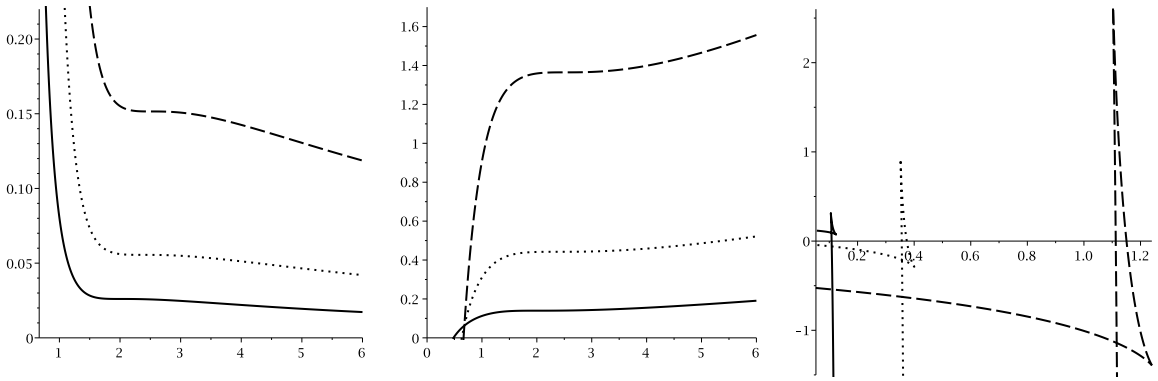

FIG. 10: $P - r_+$ (left), $T - r_+$ (middle) and $G - T$ (right) diagrams for $\beta = 0.5$, $q = 1$, $\alpha = 0.8$, $c = c_1 = c_2 = 2$, $c_3 = 0.2$, $c_4 = -0.2$, $d = 6$, $m = 0$ (continuous line), $m = 0.5$ (dotted line) and $m = 1$ (dashed line).
$P - r_+$ diagram for $T = T_c$, $T - r_+$ diagram for $P = P_c$ and $G - T$ diagram for $P = 0.5P_c$.

parameter, the black holes present a Schwarzschild like behavior and the effects of nonlinearity increases drastically. Interestingly, in case of these black holes, due to their structures, the critical behaviors are not highly modified for variation of the nonlinearity parameter comparing to massive and GB parameters (see tables $1 - 3$ for more details).

Critical temperature and pressure were highly sensitive to variation of the massive parameter. Whereas in case of the critical horizon radius, it has considerable modification due to variation of GB parameter.

Interestingly for small values of GB parameter, there exists a second order phase transition and the usual van der Waals like liquid/gas phase transition (Fig. 9). On the other hand, for specific range of GB parameter, black holes enjoy two critical horizon radii which are increasing functions of this parameter. Critical temperature and pressure for smaller critical horizon radius are increasing functions of GB parameter whereas in case of larger horizon radius, they are decreasing functions of it (see table 1).

In case of smaller critical horizon radius a negative pressure is obtained. Plotted phase diagrams represent inverse van der Waals like diagrams. In other words, the existence of swallow-tail, subcritical isobars and inflection point are observed in $G - T$, $T - r_+$ and $P - r_+$, respectively. But the behavior of diagrams before and after critical point is opposite of van der Waals like diagrams (Fig. 13). On the other hand, all the critical parameters in case of larger critical horizon radius are positive. But here, instead of swallow-tail, a cusp is observed which represents the existence of the first order phase transition (Fig. 14).

Next, for large values of α, one critical horizon radius with corresponding positive and negative critical temperature and pressure, respectively, is found. The plotted phase diagrams are similar to the ones that were observed for smaller critical point in previous case. In other words, around critical points opposite behavior to the case of van der Waals like black holes is observed (Fig. 15).

Clearly, the type of phase transition is different for the three cases that were observed in plotted phase diagrams.

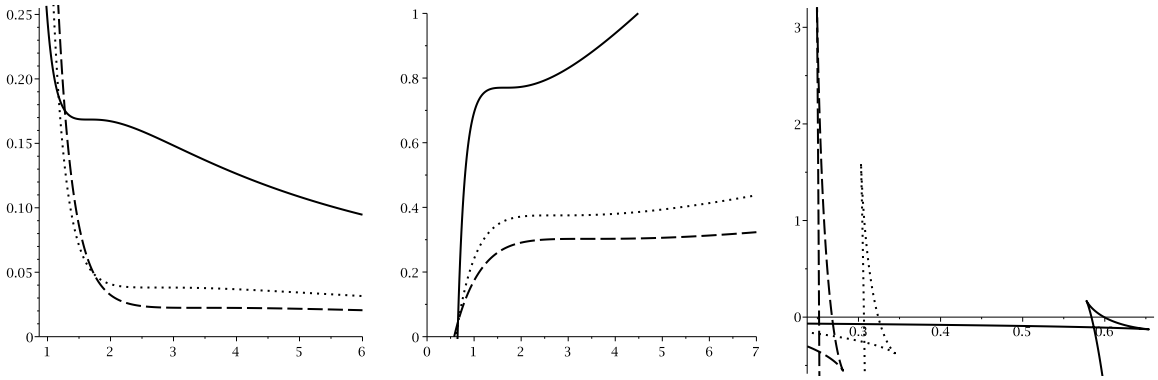

FIG. 11: $P - r_+$ (left), $T - r_+$ (middle) and $G - T$ (right) diagrams for $\beta = 0.5$, $q = 1$, $m = 0.5$, $c = c_1 = c_2 = 2$, $c_3 = 0.2$, $c_4 = -0.2$, $d = 6$, $\alpha = 0$ (continuous line), $\alpha = 0.8$ (dotted line) and $\alpha = 1.4$ (dashed line).
$P - r_+$ diagram for $T = T_c$, $T - r_+$ diagram for $P = P_c$ and $G - T$ diagram for $P = 0.5P_c$.

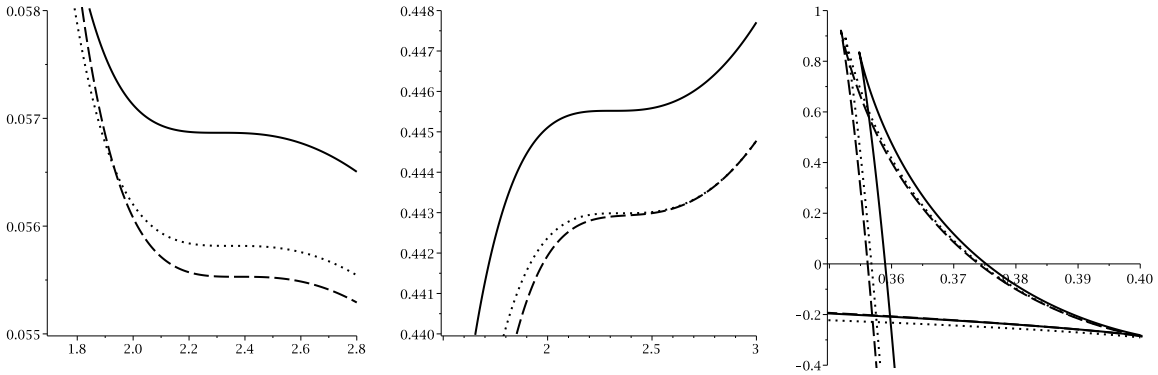

FIG. 12: $P - r_+$ (left), $T - r_+$ (middle) and $G - T$ (right) diagrams for $\alpha = 0.5$, $q = 1$, $m = 0.5$, $c = c_1 = c_2 = 2$, $c_3 = 0.2$, $c_4 = -0.2$, $d = 6$, $\beta = 10^{-9}$ (continuous line), $\beta = 0.1$ (dotted line) and $\beta = 5$ (dashed line).
$P - r_+$ diagram for $T = T_c$, $T - r_+$ diagram for $P = P_c$ and $G - T$ diagram for $P = 0.5P_c$.

The cases of two horizon radii represents a boundary case. Here, the second order phase transition is vanished, a first order phase transition and another type of phase transition is observed. Increasing GB parameter leads to vanishing the first order phase transition and the existence of other mentioned phase transition.

The GB parameter is a free parameter which represents the power of higher derivative gravity. It is evident that depending on the gravitational power, the type and number of the phase transition may vary. The phase structure of these black holes with this specific configuration (GB-BI-massive) goes under three modifications. These modifications and their corresponding properties are determined by the value of GB parameter. In other words, observed critical behaviors are functions of power of gravity.

VII. CLOSING REMARKS

In this paper, we have generalized Einstein-BI gravity by considering GB and massive gravities. It was shown that obtained black hole solutions in this case can enjoy the existence of multiple horizons. Considering the configurations of the horizon, different phenomenologies could be described. Conserved and thermodynamic quantities, that were calculated for these black holes, satisfied the first law of thermodynamics.

Next, we studied thermal stability of these black holes and their corresponding phase transition in the context of canonical ensemble. We also investigated the effects of different parameters on the behavior of the temperature. We found that considering the contributions of different parameters, the behavior of the temperature could be highly modified and resulted into different number of phase transitions, hence, different stability conditions.

It was seen that in case of three divergencies for the heat capacity, GB and massive parameters has opposing effects, although the existence of three phase transitions were observed for specific values of α. On the other hand, strong

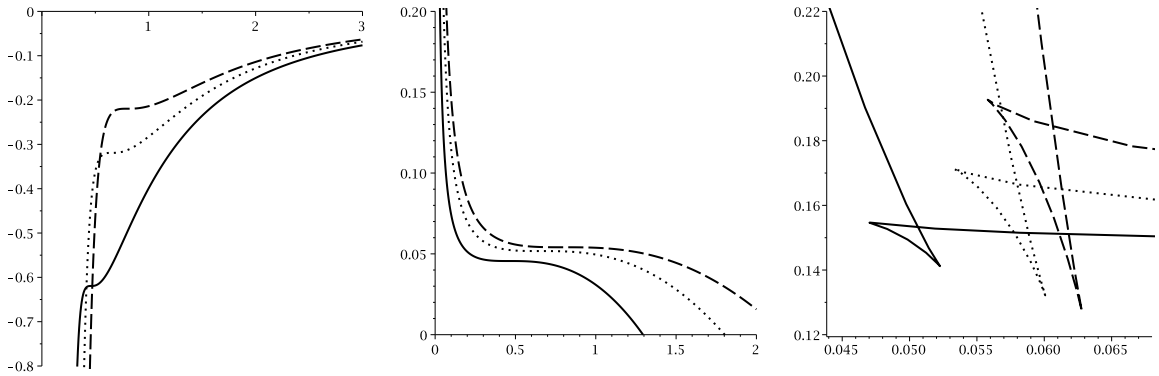

FIG. 13: $P - r_+$ (left), $T - r_+$ (middle) and $G - T$ (right) diagrams for $\beta = 0.5$, $q = 1$, $m = 0.5$, $c = c_1 = c_2 = 2$, $c_3 = 0.2$, $c_4 = -0.2$, $d = 6$, $\alpha = 7$ (continuous line), $\alpha = 8$ (dotted line) and $\alpha = 9$ (dashed line).
$P - r_+$ diagram for $T = T_c$, $T - r_+$ diagram for $P = P_c$ and $G - T$ diagram for $P = 0.5P_c$, *For smaller roots.*

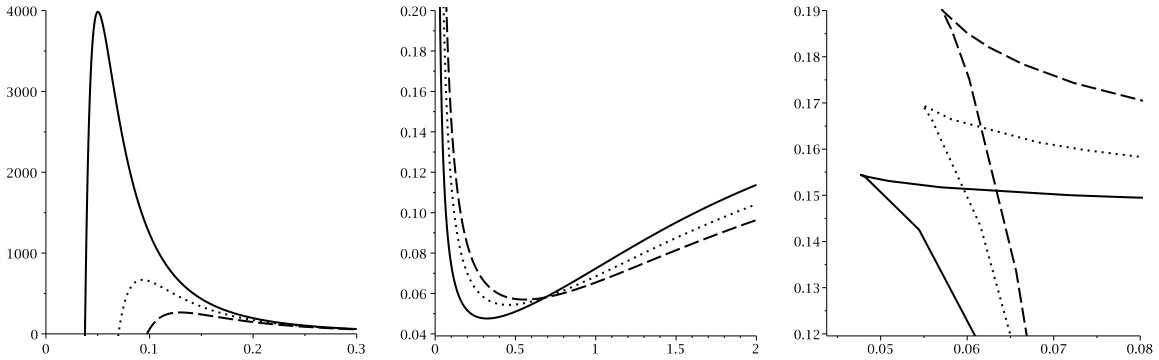

FIG. 14: $P - r_+$ (left), $T - r_+$ (middle) and $G - T$ (right) diagrams for $\beta = 0.5$, $q = 1$, $m = 0.5$, $c = c_1 = c_2 = 2$, $c_3 = 0.2$, $c_4 = -0.2$, $d = 5$, $\alpha = 7$ (continuous line), $\alpha = 8$ (dotted line) and $\alpha = 9$ (dashed line).
$P - r_+$ diagram for $T = T_c$, $T - r_+$ diagram for $P = P_c$ and $G - T$ diagram for $P = 0.5P_c$, *For larger roots.*

nonlinearity parameter modified the behavior of the temperature completely. A region of non-physical and phase transitions related to root and four divergencies were observed.

It is evident that matter field (nonlinear electrodynamics), gravitational field (GB gravity) and massive gravity contribute highly to thermodynamical structure of these black holes. Each of these factors add an effective parameter to the phase transitions and thermal stability structure of these black holes which enable one to modify/control the effects of other parameters.

It was also pointed out that dimensionality modifies the stability and thermodynamical behavior of the system. The cases of $d < 7$ and $d > 7$ had different behaviors regarding stability conditions. These conditions were originated from number of roots and divergencies in the heat capacity. The case of $d = 7$ was also different from the other dimensions.

Here, we should point out that in cases of the maximums in temperature, a phase transition from larger unstable to smaller stable exists. Whereas, for minimums of the temperature smaller unstable to larger stable phase transition takes place which shows that temperature itself presents an independent picture for studying phase transitions and stability conditions.

Next, we have studied the critical behavior of the GB-BI-massive black holes through $P - V$, $T - V$ and $G - T$ diagrams. We employed the analogy and linear proportionality between cosmological constant and thermodynamical pressure in extended phase space. It was shown that variation of m, α and β affect the critical values, phase transition region and size of the swallow-tail shape. The variation of the GB parameter leads to interesting second order, first order and another type of phase transition. The case of the second order phase transition was related to existence of usual van der Waals like behavior. Whereas, first order phase transition was due to existence of cusp. The other type of phase transition was for the cases in which around the phase transition point, the behavior of the system was opposite (and also symmetric) to the van der Waals manner. Therefore, three different behaviors were observed around critical points for these black holes. Considering these three behaviors around the critical points, one can

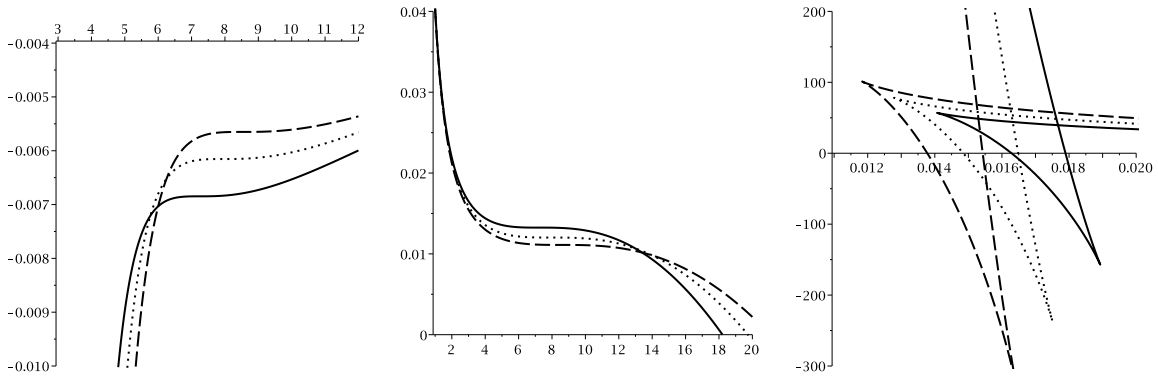

FIG. 15: $P - r_+$ (left), $T - r_+$ (middle) and $G - T$ (right) diagrams for $\beta = 0.5$, $q = 1$, $m = 0.5$, $c = c_1 = c_2 = 2$, $c_3 = 0.2$, $c_4 = -0.2$, $d = 5$, $\alpha = 400$ (continuous line), $\alpha = 500$ (dotted line) and $\alpha = 600$ (dashed line).
$P - r_+$ diagram for $T = T_c$, $T - r_+$ diagram for $P = P_c$ and $G - T$ diagram for $P = 0.5P_c$.

conclude that in strong higher derivative gravity the phase structure of these black holes will be drastically different and the behavior of the system will be even opposite of the van der Waals behavior. To our knowledge, this is a unique behavior which is observed only for these black holes, yet.

Considering obtained three types of phase transition, it will be worthwhile to study these phase transitions in context of superconductors. Also, it will be interesting to study the structure of new phase transition that was observed in this paper in more details.

Acknowledgments

We thank Shiraz University Research Council. This work has been supported financially by the Research Institute for Astronomy and Astrophysics of Maragha, Iran.

[1] S. Perlmutter, et al., Astrophys. J. **517**, 565 (1999);
S. Perlmutter, et al., Phys. Rev. Lett. **83**, 670 (1999);
A. G. Riess, et al., Astrophys. J. **607**, 665 (2004).
[2] A. T. Lee et al., Astrophys. J. **561**, L1 (2001);
C. B. Netterfield et al., Astrophys. J. **571**, 604 (2002);
N. W. Halverson et al., Astrophys. J. **568**, 38 (2002);
D. N. Spergel et al., Astrophys. J. Suppl. **148**, 175 (2003).
[3] N. Arkani-Hamed, S. Dimopoulos, and G. Dvali, Phys. Lett. B **429**, 263 (1998);
I. Antoniadis, N. Arkani-Hamed, S. Dimopoulos, and G. Dvali, Phys. Lett. B **436**, 257 (1998).
L. Randall and R. Sundrum, Phys. Rev. Lett. **83**, 3370 (1999);
G. Dvali, G. Gabadadze, and M. Porrati, Phys. Lett. B **485**, 208 (2000);
G. Dvali, G. Gabadadze, and M. Shifman, Phys. Rev. D **67**, 044020 (2003).
[4] D. Ida, JHEP **09**, 014 (2000);
J. M. Cline and H. Firouzjahi, Phys. Rev. D **64**, 023505 (2001);
P. Brax and C. Van de Bruck, Class. Quantum Gravit. **20**, 201R (2003);
S. Mizuno, S. J. Lee and E. J. Copeland, Phys. Rev. D **70**, 043525 (2004);
T. Nihei, N. Okada and O. Seto, Phys. Rev. D **71**, 063535 (2005).
[5] C. Brans and R. H. Dicke, Phys. Rev. **124**, 925 (1961);
R. V. Wagoner, Phys. Rev. D **1,** 3209 (1970);
C. M. Will, Phys. Rev. D **50**, 6058 (1994);
S. J. Kolitch and D. M. Eardley, Ann. Phys. **241**, 128 (1995);
C. Barrabes and G. F. Bressange, Class. Quantum Gravit. **14**, 805 (1997);
D. I. Santiago, D. Kalligas and R. V. Wagoner, Phys. Rev. D **56**, 7627 (1997);
C. A. Clarkson, A. A. Coley and E. S. D. O'Neill, Phys. Rev. D **64**, 063510 (2001);
S. Capozziello and A. Troisi, Phys. Rev. D **72**, 044022 (2005);
T. P. Sotiriou, Class. Quantum Gravit. **23**, 5117 (2006);

S. F. Wu, G. H. Yang and P. M. Zhang, Prog. Theor. Phys. **120**, 615 (2008).
[6] S. Capozziello, V. F. Cardone and M. Francaviglia, Gen. Relativ. Gravit. **38**, 711 (2006);
T. Chiba, T. L. Smith and A. L. Erickcek, Phys. Rev. D **75**, 124014 (2007);
L. Amendola, R. Gannouji, D. Polarski, and S. Tsujikawa, Phys. Rev. D **75**, 083504 (2007);
G. Cognola, E. Elizalde, S. Nojiri, S. D. Odintsov, L. Sebastiani and S. Zerbini, Phys. Rev. D **77**, 046009 (2008);
A. D. Felice and S. Tsujikawa, Living Rev. Rel. **13**, 3 (2010);
T. P. Sotiriou, and V. Faraoni, Rev. Mod. Phys. **82**, 451 (2010);
G. J. Olmo and D. Rubiera-Garcia, Phys. Rev. D **84**, 124059 (2011).
[7] S. H. Hendi, B. Eslam Panah and M. Mousavi, Gen. Relativ. Gravit. **44**, 835 (2012);
S. H. Hendi, R. B. Mann, N. Riazi, and B. Eslam Panah, Phys. Rev. D **86**, 104034 (2012);
J. Q. Guo and A. V. Frolov, Phys. Rev. D **88**, 124036 (2013);
I. D. Martino, M. D. Laurentis, F. Atrio-Barandela and S. Capozziello, MNRAS **442**, 921 (2014);
S. H. Hendi, B. Eslam Panah and C. Corda, Can. J. Phys. **92**, 1 (2014);
J. Q. Guo, D. Wang and A. V. Frolov, Phys. Rev. D **90**, 024017 (2014);
S. H. Hendi, B. Eslam Panah and R. Saffari, Int. J. Mod. Phys. D **23**, 1450088 (2014).
[8] D. Lovelock, J. Math. Phys. **12**, 498 (1971);
D. Lovelock, J. Math. Phys. **13**, 874 (1972).
[9] S. Chakraborty, JHEP **08**, 029 (2015).
[10] S. Chakraborty and T. Padmanabhan, Phys. Rev. D **90**, 084021 (2014).
[11] T. Padmanabhan and D. Kothawala, Phys. Rept. **531**, 115 (2013).
[12] B. Zwiebach, Phys. Lett. B **156**, 315 (1985);
D. G. Boulware and S. Deser, Phys. Rev. Lett. **55**, 2656 (1985).
[13] A. H. Chamseddine, Phys. Lett. B **233**, 291 (1989);
F. Muller-Hoissen, Nucl. Phys. B **349**, 235 (1990).
[14] G. Pastras and D. Manolopoulos, JHEP **11**, 007 (2014).
[15] Y. P. Hu, P. Sun and J. H. Zhang, Phys. Rev. D **83**, 126003 (2011);
Y. P. Hu, H. F. Li and Z. Y. Nie, JHEP **01**, 123 (2011).
[16] M. Born and L. Infeld, Proc. Roy. Soc. Lon. **144**, 425 (1934).
[17] B. Hoffmann, Phys. Rev. **47**, 877 (1935).
[18] E. S. Fradkin and A. A. Tseytlin, Phys. Lett. B **163**, 123 (1985);
D. L. Wiltshire, Phys. Rev. D **38**, 2445 (1988);
R. G. Leigh, Mod. Phys. Lett A **4**, 2767 (1989);
M. Cataldo and A. Garcia, Phys. Lett. B **456**, 2833 (1999);
G. W. Gibbons and C. A. R. Herdeiro, Class. Quantum Gravit. **18**, 1677 (2001).
[19] S. Fernando and D. Krug, Gen. Relativ. Gravit. **35**, 129 (2003);
D. J. Cirilo-Lombardo, Gen. Relativ. Gravit. **37**, 847 (2005);
M. H. Dehghani and H. R. Rastegar Sedehi, Phys. Rev. D **74**, 124018 (2006);
Y. S. Myung, Y. W. Kim and Y. J. Park, Phys. Rev. D **78**, 044020 (2008);
O. Miskovic and R. Olea, Phys. Rev. D **77**, 124048 (2008);
S. H. Hendi, JHEP **03**, 065 (2012);
H. S. Ramadhan, B. A. Cahyo and M. Iqbal, Phys. Rev. D **92**, 024021 (2015);
F. Atamurotov, S. G. Ghosh and B. Ahmedov, [arXiv:1506.03690].
[20] G. W. Gibbons, Rev. Mex. Fis. **49**, 19 (2003).
[21] M. Fierz, Helv. Phys. Acta **12**, 3 (1939);
M. Fierz and W. Pauli, Proc. Roy. Soc. Lond. A **173**, 211 (1939).
[22] D. G. Boulware and S. Deser, Phys. Rev. D **6**, 3368 (1972).
[23] S. F. Hassan and R. A. Rosen, Phys. Rev. Lett. **108**, 041101 (2012);
S. F. Hassan, R. A. Rosen and A. Schmidt-May, JHEP **02**, 026 (2012).
[24] P. Minjoon, Class. Quantum Gravit. **28**, 105012 (2011).
[25] C. de Rham and G. Gabadadze, Phys. Rev. D **82**, 044020 (2010);
C. de Rham, G. Gabadadze and A. J. Tolley, Phys. Rev. Lett. **106**, 231101 (2011);
K. Hinterbichler, Rev. Mod. Phys. **84**, 671 (2012).
[26] Y. F. Cai, D. A. Easson, C. Gao and E. N. Saridakis, Phys. Rev. D **87**, 064001 (2013);
E. Babichev and A. Fabbri, JHEP **07**, 016 (2014).
[27] E. Babichev, C. Deffayet and R. Ziour, Phys. Rev. Lett. **103**, 201102 (2009);
L. Alberte, A. H. Chamseddine and V. Mukhanov, JHEP **12**, 023 (2010);
K. Koyama, G. Niz and G. Tasinato, Phys. Rev. Lett. **107**, 131101 (2011);
T. M. Nieuwenhuizen, Phys. Rev. D **84**, 024038 (2011);
M. S. Volkov, Class. Quantum Gravit. **30**, 184009 (2013);
E. Babichev and C. Deffayet, Class. Quantum Gravit. **30**, 184001 (2013).
[28] D. Vegh, [arXiv:1301.0537].
[29] S. F. Hassan and R. A. Rosen, JHEP **07**, 009 (2011).
[30] T. Andrade and B. Withers, [arXiv:1311.5157];
M. Taylor and W. Woodhead, [arXiv:1406.4870];

M. Baggioli and O. Pujolas, Phys. Rev. Lett. **114**, 251602 (2015);
M. Baggioli and D. K. Bratta, [arXiv:1504.07635].
[31] R. G. Cai, Y. P. Hu, Q. Y. Pan and Y. L. Zhang, Phys. Rev. D **91**, 024032 (2015).
[32] J. Xu, L. M. Cao and Y. P. Hu, Phys. Rev. D **91**, 124033 (2015).
[33] S. H. Hendi , S. Panahiyan, B. Eslam Panah and M. Momennia, [arXiv:1506.07262].
[34] S. H. Hendi, S. Panahiyan and B. Eslam Panah, [arXiv:1507.06563].
[35] S. H. Hendi, B. Eslam Panah and S. Panahiyan, [arXiv:1508.01311].
[36] R. A. Davison, Phys. Rev. D **88**, 086003 (2013);
M. Blake and D. Tong, Phys. Rev. D **88**, 106004 (2013);
R. A. Davison, K. Schalm and J. Zaanen, Phys. Rev. B **89**, 245116 (2014).
[37] Y. S. Myung, Phys. Rev. D **77**, 104007 (2008);
B. M. N. Carter and I. P. Neupane, Phys. Rev. D **72**, 043534 (2005);
D. Kastor, S. Ray and J. Traschen, Class. Quantum Gravit. **26**, 195011 (2009);
F. Capela and G. Nardini, Rev. D **86**, 024030 (2012).
[38] J. Creighton and R. B. Mann, Phys. Rev. D **52**, 4569 (1995);
G. W. Gibbons, R. Kallosh and B. Kol, Phys. Rev. Lett. **77**, 4992 (1996);
B. P. Dolan, Class. Quantum Gravit. **28**, 125020 (2011);
B. P. Dolan, Class. Quantum Gravit. **28**, 235017 (2011).
[39] S. H. Hendi, S. Panahiyan and R. Mamasani, Gen. Relativ. Gravit. **47**, 91 (2015).
[40] D. Kubiznak and R. B. Mann, JHEP **07**, 033 (2012);
R. G. Cai, L. M. Cao, L. Li and R. Q. Yang, JHEP **09**, 005 (2013);
M. B. Jahani Poshteh, B. Mirza and Z. Sherkatghanad, Phys. Rev. D **88**, 024005 (2013);
S. Chen, X. Liu and C. Liu, Chin. Phys. Lett. **30**, 060401 (2013);
S. H. Hendi and M. H. Vahidinia, Phys. Rev. D **88**, 084045 (2013);
J. X. Mo and W. B. Liu, Eur. Phys. J. C **74**, 2836 (2014);
D. C. Zou, S. J. Zhang and B. Wang, Phys. Rev. D **89**, 044002 (2014);
W. Xu and L. Zhao, Phys. Lett. B **736**, 214 (2014);
S. H. Hendi, S. Panahiyan and B. Eslam Panah, [arXiv:1410.0352].
J. Xu, L. M. Cao and Y. P. Hu, Phys. Rev. D **91**, 124033 (2015);
S. H. Hendi, S. Panahiyan and M. Momennia, [arXiv:1503.03340]
E. Caceres, P. H. Nguyen and J. F. Pedrazab, [arXiv:1507.06069].
S. H. Hendi, S. Panahiyan and B. Eslam Panah, *to appear in PTEP*.
[41] D. Kastor, S. Ray and J. Traschen, Class. Quantum Gravit. **26**, 195011 (2009);
C. V. Johnson, Class. Quantum Gravit. **31**, 205002 (2014);
B. P. Dolan, JHEP **10**, 179 (2014);
B. P. Dolan, Mod. Phys. Lett. A **30**, 1540002 (2015).
[42] E. Caceres, P. H. Nguyen and J. F. Pedraza, [arXiv:1507.06069].
[43] D. L. Wiltshire, Phys. Rev. D **38**, 2445 (1988);
M. Aiello, R. Ferraro and G. Giribet, Phys. Rev. D **70**, 104014 (2004);
M. H. Dehghani and S. H. Hendi, Int. J. Mod. Phys. D **16**, 1829 (2007).
[44] J. D. Beckenstein, Phys. Rev. D **7**, 2333 (1973);
S. W. Hawking and C. J. Hunter, Phys. Rev. D **59**, 044025 (1999);
C. J. Hunter, Phys. Rev. D **59**, 024009 (1999);
S. W. Hawking, C. J. Hunter and D. N. Page, Phys. Rev. D **59**, 044033 (1999).
[45] J. E. Kim, B. Kyae and H. M. Lee, Phys. Rev. D **62**, 045013 (2000);
Y. M. Cho and I. P. Neupane, Phys. Rev. D **66**, 024044 (2002);
C. Charmousis and J. F. Dufaux, Class. Quantum Gravit. **19**, 4671 (2002);
G. Kofinas, R. Maartens and E. Papantonopoulos, JHEP **10**, 066 (2003);
R. G. Cai and Q. Guo, Phys. Rev. D **69**, 104025 (2004);
A. Barrau, J. Grain and S. O. Alexeyev, Phys. Lett. B **584**, 114 (2004);
K. I. Maeda and T. Torii, Phys. Rev. D **69**, 024002 (2004);
C. de Rham and A. J. Tolley, JCAP **07**, 004 (2006);
G. Dotti, J. Oliva and R. Troncoso, Phys. Rev. D **76**, 064038 (2007);
R. A. Brown, Gen. Relativ. Gravit. **39**, 477 (2007);
H. Maeda, V. Sahni and Y. Shtanov, Phys. Rev. D **76**, 104028 (2007);
C. Charmousis, Lect. Notes Phys. **769**, 299 (2009);
S. H. Hendi and B. Eslam Panah, Phys. Lett. B **684**, 77 (2010);
M. Bouhmadi-Lopez, Y. W. Liu, K. Izumi and P. Chen, Phys. Rev. D **89**, 063501 (2014);
S. H. Hendi, S. Panahiyan and E. Mahmoudi, Eur. Phys. J. C **74**, 3079 (2014);
Y. Yamashita and T. Tanaka, JCAP **06**, 004 (2014);
A. Maselli, P. Pani, L. Gualtieri and V. Ferrari, [arXiv:1507.00680].